Investigating δ^{13}C values in stalagmites from tropical South America for the last two millennia

Valdir Felipe Novello [a, *], Francisco William da Cruz [a], Mathias Vuille [b], José Leandro Pereira Silveira Campos [a], Nicolás Misailidis Stríkis [c], James Apaéstegui [d], Jean Sebastien Moquet [e], Vitor Azevedo [a], Angela Ampuero [a], Giselle Utida [a], Xianfeng Wang [f], Gustavo Macedo Paula-Santos [g], Plinio Jaqueto [h], Luiz Carlos Ruiz Pessenda [i], Daniel O. Breecker [j], Ivo Karmann [a]

[a] *Institute of Geosciences, University of São Paulo, São Paulo, 05508-080, Brazil*
[b] *Department of Atmospheric and Environmental Sciences, University at Albany, Albany, 12222, USA*
[c] *Departamento de Geoquímica, Universidade Federal Fluminense, Niterói, 24020-141, Brazil*
[d] *Instituto Geofísico del Perú, Lima, 15012, Peru*
[e] *Institut des Sciences de la Terre d'Orléans, Orléans, 45100, France*
[f] *Asian School of the Environment and Earth Observatory of Singapore, Nanyang Technological University, 639798 Singapore*
[g] *Institute of Geoscience University of Campinas, 13083-855, Brazil*
[h] *Instituto de Astronomia, Geofísica e Ciências Atmosféricas, University of São Paulo, São Paulo, 05508-090, Brazil*
[i] *Center for Nuclear Energy in Agriculture (CENA), University of São Paulo, São Paulo, 13416-000, Brazil*
[j] *Jackson School of Geosciences, University of Texas, Austin, 2305, USA*

ARTICLE INFO

ABSTRACT

Due to the many factors controlling δ^{13}C values in stalagmites, complicating their paleoclimatic and paleoenvironmental interpretation, most studies do not present δ^{13}C values, but instead focus mainly on δ^{18}O values. This is also the case for most cave studies from tropical South America, where many new δ^{18}O stalagmite records covering the last millennia were recently published. Here, we review the δ^{13}C values in stalagmites, investigating the influence on this proxy of local hydroclimate, altitude, temperature and vegetation types, by employing a new dataset composed of published and unpublished carbon isotope records from various sites in tropical South America. The main factors influencing δ^{13}C values are associated with the local hydroclimate, followed by minor effects from temperature. Most of the isotopic records show a significant correlation between the δ^{13}C and δ^{18}O values, indicating a close relationship between local hydroclimate and atmospheric convective processes related to the South American Monsoon System.

© 2021 Elsevier Ltd. All rights reserved.

1. Introduction

Measurements of carbon isotope (δ^{13}C) ratios are essential for (paleo)environmental studies, such as those regarding the carbon cycle, past food consumption by pre-historic societies, paleo-vegetation reconstructions, soil dynamics, aspects regarding animal migration and food consumption, etc. (Rayner et al., 1999; Calo and Cortés, 2009; Pansani et al., 2019; Novello et al., 2019).

However, δ^{13}C values of speleothems are generally considered difficult to interpret and, in most cases, are not reported in isotopic studies based on speleothems. Studies from tropical South America, in particular, have almost completely neglected δ^{13}C values from stalagmites and instead relied solely on δ^{18}O values for reconstruction of the South American Monsoon System (SAMS) (Reuter et al., 2009; Novello et al., 2012, 2016, 2018; 2018; Apaéstegui et al., 2014, 2018; Vuille et al., 2012; Kanner et al., 2013; Wang et al., 2017). Here we present a compilation of 25 δ^{13}C records (13 of them hitherto unpublished) from stalagmites collected at different sites throughout tropical South America and covering the last two millennia (referred to here as the δ^{13}C_2k_SA dataset) with

aims to revise and characterize the main factors controlling $\delta^{13}C$ variability in these stalagmites and provide possible paleoclimate and paleoenvironmental reconstructions for the region.

In Section 2 we review the mechanisms that control the $\delta^{13}C$ values in the stalagmites and the related global and regional forcings. In Section 3 we present the data, the stalagmites, the study sities and methods. In Section 4 we show the results (data set) and in Section 5 we discuss the interpretations of the new records and their regional relationships. Additionally, using Principal Component Analysis (PCA), we propose a new hydrological index for South America based on the $\delta^{13}C\_2k\_SA$ dataset.

2. Background

2.1. Main processes controlling $\delta^{13}C$ values in speleothems

The initial source of carbon for speleothems is the CO_2 present in the soil, mainly provided by plant roots' respiration and decomposition of organic matter. It forms carbonic acid in contact with water, which dissolves cave host-rock (limestones or dolostones) according to the equation:

$$CaCO_3 + H_2O + CO_2 \leftrightarrow Ca^{2+} + 2HCO_3^-. \quad (1)$$
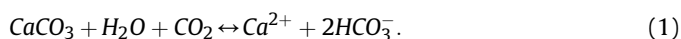
Open and closed system models were proposed to explain two extreme cases of dissolution of calcium carbonate in the percolating solution (Fohlmeister et al., 2011; McDermott et al., 2004; Hendy, 1971). In an open system, the percolating solution remains in equilibrium with the infinite reservoir of soil CO_2 and, thereby, the bicarbonate in solution receives the $\delta^{13}C$ fingerprint of this reservoir. Under these conditions, the contribution of the $\delta^{13}C$ values from the bedrock to the HCO_3^- in solution can be neglected. In a closed system, during the percolation into the epikarst, the solution loses contact with the soil CO_2, and the CO_2 in solution is progressively consumed through the dissolution of the bedrock. The rock dissolution is limited by the initial amount of CO_2 and, consequently, through this process the $\delta^{13}C$ from the bedrock influences the isotopic composition of the remaining solution (McDermott, 2004). In most caves, the interaction between the percolation solution and the host-rock occurs as an intermediate way between open and closed systems.

The $\delta^{13}C$ values in pedogenic carbonate are closely related to the isotopic values from the surrounding vegetation (Cerling, 1984; Quade et al., 1989), defined by the plant type (C_3, C_4 or CAM), which in turn, will be conditioned by climatic parameters such as temperature, pluviosity, rainfall seasonality and atmospheric CO_2 (Ehleringer et al., 1997). Vegetation dominated by C_3 plants has $\delta^{13}C$ values between −32‰ and −20‰, while vegetation dominated by C_4 plants is characterized by values between −17‰ and −9‰ (Badeck et al., 2015). CAM plants have $\delta^{13}C$ values that overlap with both C_3 and C_4 plants. In addition, $\delta^{13}C$ values of individual C_3 plant species can vary approximately 1−2‰, depending on water availability (e.g., Hartman and Danin, 2010). The differences in the $\delta^{13}C$ values from total organic matter in soil resulting from the dominant plant types are transferred to stalagmites precipitated under their respective environment. Thus, stalagmites precipitated in caves under conditions dominated by C_3 plants typically have values ranging from −14‰ to −6‰, while those forming below C_4 plant cover range from −6‰ to +2‰ (McDermott, 2004; Baker et al., 1997; Dreybrodt, 1988). Variations in soil $\delta^{13}C$ values and their evolution over time are controlled by carbon inputs from vegetation, which is proportional to the organic matter amount and vegetation density; thus denser vegetation is also associated with more depleted values in soil $\delta^{13}C$ and vice-versa (Pessenda et al., 2020). However, the presence of CAM plants can complicate this interpretation since this type of plant present a large range of $\delta^{13}C$ values. In addition, the $\delta^{13}C$ values of C_3 plants are sensitive to atmospheric CO_2 levels (Van de Water et al., 1994; Schubert and Jahen, 2012), producing a signal that is transferred to stalagmites (Breecker, 2017).

In the cave system, $\delta^{13}C$ values from dissolved inorganic carbon (DIC) can undergo fractionation through prior calcite precipitation (PCP), which is forced by CO_2 degassing that preferentially removes ^{12}C from the solution to the cave atmosphere (Mickler et al., 2019), depleting ^{12}C from the final isotopic product recorded in stalagmites (Baker et al., 1997). PCP increases during drier periods due to the increased exposure of seepage solution to air. This can occur during the contact of the solution with air pockets along the epikarst flow routes and/or with the increase of dripping interval, where the solution is exposed to the cave air for longer time at the stalactites; both results in CO_2 degassing from the solution, promoting the carbonate precipitation in the epikarst and/or stalactites with higher $\delta^{13}C$ values (Fairchild and Baker, 2012). Therefore, the variations in the PCP rate are climate related. In monsoonal climates, such as in (sub)tropical South America, the amount effect is the dominant process that affects the $\delta^{18}O$ value of rainwater, such that an increase in the amount of rainfall results in waters with lower $\delta^{18}O$ values (Vuille et al., 2012). This increase in rainfall amount might also cause a decrease in the $\delta^{13}C$ value of speleothem calcite, by increasing the soil moisture content and soil respiration rates or by reducing PCP, resulting in a positive correlation between the $\delta^{18}O$ and $\delta^{13}C$ values of speleothem calcite/aragonite (Cruz et al., 2006; Mickler et al., 2006; and references therein). While $\delta^{13}C$ and $\delta^{18}O$ values may be correlated for different reasons, high correlation between both isotopic ratios can also be indicative of forced kinetic fractionation, since carbon and oxygen are fractioned in the same direction in this process (Hendy et al., 1971). The isotopic disequilibrium increases with enhanced ventilation of the cave, which depends on the temperature gradient between the air inside and outside of the cave. However, the range of values resulting from the fractionation factor between $CaCO_3$ and HCO_3^- in tropical temperatures of 15−30°C has been documented to be < 0.5‰ (Polag et al., 2010 and references therein). Recently, Fohlmeister et al. (2020), using a large dataset of $\delta^{13}C$ values in stalagmites deposited post-1900 CE, show evidence for a temperature control on this proxy, likely driven by vegetation and soil processes, while PCP can explain the wide $\delta^{13}C$ range observed for concurrently deposited samples from the same cave.

2.2. Processes controlling the $\delta^{13}C$ values in speleothems from South America

The main mode of climate variability in tropical South America is defined by the SAMS behavior, which also influences vegetation changes. Most of the $\delta^{18}O$ records from stalagmites in South America show a weak monsoon activity during the Medieval Climate Anomaly (MCA, 900−1100 years CE), in contrast with a strong activity during the Little Ice Age (LIA, 1600−1850 years CE) (Bird et al., 2011; Vuille et al., 2012; Novello et al., 2016, 2018). During the LIA period, a moisture dipole was documented between the eastern and western portions of tropical South America, due to the displacement of the South Atlantic Convergence Zone (SACZ) toward the southwest (Campos et al., 2019; Novello et al., 2018). This change in climate is still not investigated with the $\delta^{13}C$ values in stalagmites.

Few studies focused on the $\delta^{13}C$ values from speleothems in South America. Cruz et al. (2006) interpreted the $\delta^{13}C$ from Botuverá cave (southeastern Brazil, point 8 in Fig. 1) as a proxy for soil CO_2 productivity, which is modulated at orbital time scales by

by the $\delta^{13}C$ and $\delta^{18}O$, respectively (Wortham et al., 2017).
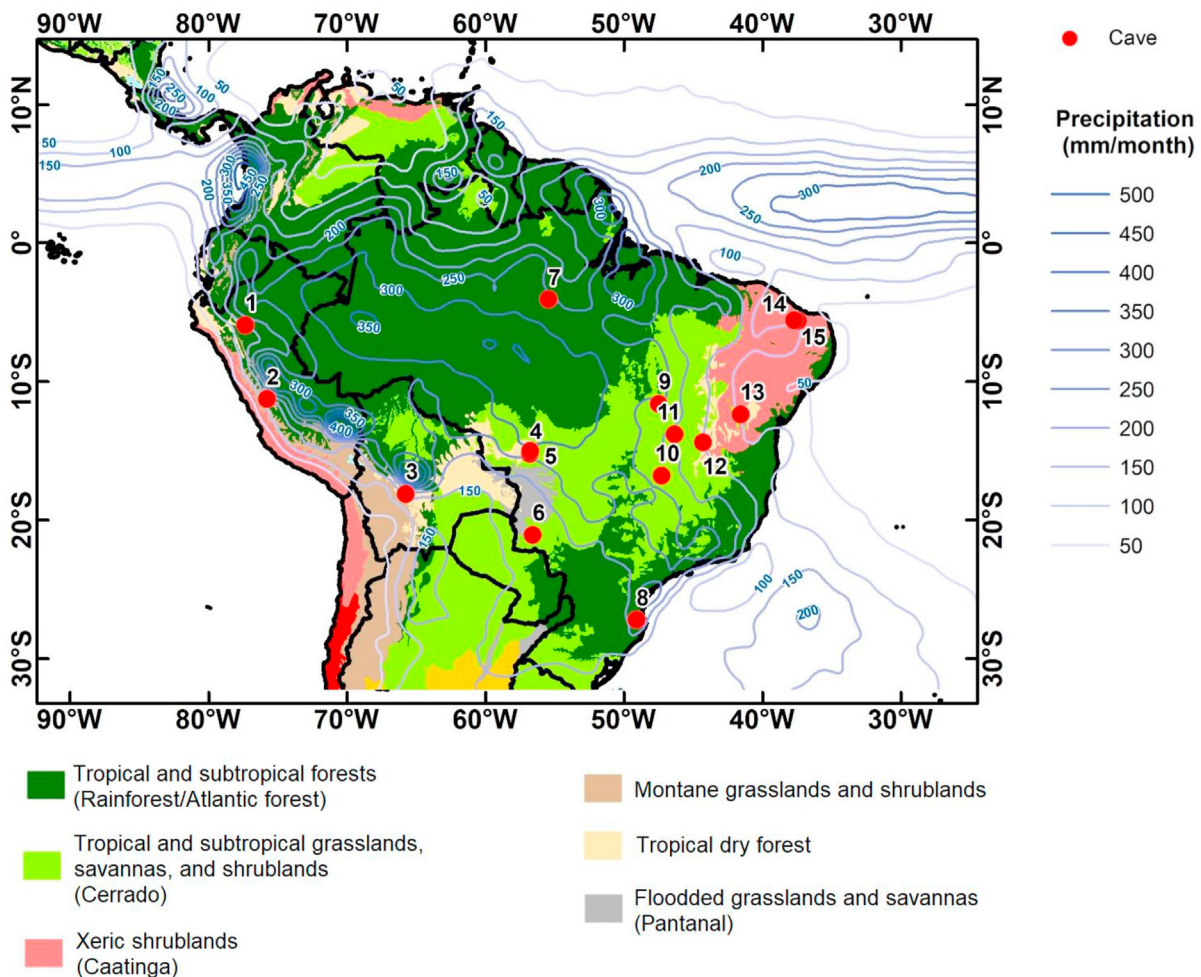
Fig. 1. Map of tropical South America with vegetation types (Olson et al., 2001), the main biomes, precipitation (blue isolines - mm/month, derived from the annual mean for the period from 1998 to 2017, with data from TRMM 3b43 — Huffman et al., 2014) and location of the study sites from the $\delta^{13}C\_2k\_SA$ dataset. 1- Huagapo cave; 2- Palestina cave; 3- Umajalanta–Chiflonkhakha; 4- Pau d'Alho cave; 5- Curupira cave; 6- Járaguá cave; 7- Paraiso cave; 8- Botuverá cave; 9- Mata Virgem cave; 10- Tamboril cave; 11- São Matheus and São Bernardo cave system; 12- Anjos cave; 13- Diva, Torrinha, Lapa Doce caves; 14- Furna Nova cave; 15- Trapiá cave. (For interpretation of the references to color in this figure legend, the reader is referred to the Web version of this article.)

changes in local temperature brought about by shifts between summer monsoonal and winter extratropical circulation. Novello et al. (2019) reported a decrease of 9‰ in the $\delta^{13}C$ values from Jaraguá cave (point 6 in Fig. 1) during the transition between the last Glacial and the Holocene periods, resulting from a combination of changes above the cave, including: changes in the predominant vegetation type from C_4 to C_3, increase of organic matter and soil horizons, which were mainly caused by the increase in temperature and atmospheric CO_2. For the last two millennia, Jaqueto et al. (2016) show that the concentration of magnetic minerals and $\delta^{13}C$ values in the ALHO6 stalagmite from Pau d'Alho cave (point 4 in Fig. 1) is governed by soil dynamics and changes in vegetation cover above the cave. Dry periods are associated with less stable soils, resulting in high erosion and increased mineral flux into karst systems, which occurs simultaneously with increasing $\delta^{13}C$ values. Conversely, wetter periods with low $\delta^{13}C$ values are associated with soils topped by denser vegetation that retains micrometer-scale pedogenic minerals and thus reduces detrital fluxes into the cave. Azevedo et al. (2019) further explored the relationship between $\delta^{13}C$ and $\delta^{18}O$ during the last millennium in a speleothem (MV3)

from the Brazilian Central region (point 9 in Fig. 1), where wetter (drier) periods are also associated with lower (higher) values of $\delta^{18}O$ and $\delta^{13}C$ and higher (lower) speleothem growth rates. The same interpretation was utilized for the $\delta^{13}C$ values of the stalagmites from Tamboril cave, located further south (point 10 in Fig. 1). However, at this site the $\delta^{18}O$ and $\delta^{13}C$ do not co-vary, which the authors interpret as a result of the decoupling between the local hydroclimate and SAMS, documented by the $\delta^{13}C$ and $\delta^{18}O$, respectively (Wortham et al., 2017).

The global increase of the atmospheric CO_2 concentration and temperature likely also influenced the $\delta^{13}C$ values of stalagmites during the last century. Since 1850 the land surface air temperature increased by about 1.44 °C (Jia et al., 2019), affecting the fractionation between the seepage solution and the carbonate precipitated inside the caves (Lachniet, 2009), as well as promoting changes in cave ventilation (Baldini et al., 2008). Furthermore, depleted isotopic carbon has been emitted into the atmosphere due to the burning of fossil fuels, thereby decreasing the atmospheric $\delta^{13}C$ value that is transferred to vegetation. The increase of atmospheric CO_2 can also favor the flourishing of C_3 plants, which are less

adapted than C_4 plants to low atmospheric CO_2 concentrations (Ehleringer et al., 1997).

3. Data material and methods

3.1. $\delta^{13}C$ data

The dataset used in this study comprises 25 speleothem $\delta^{13}C$ records, of which 13 were hitherto unpublished. $\delta^{18}O$ records and chronological models have been published for all stalagmite records. Data from the published records were obtained from the supplementary material of the respective papers or downloaded from the NOAA speleothem database (http://www.ncdc.noaa.gov/data-access/paleoclimatology-data/datasets/speleothem). Our main goal with this study is to introduce new cave records to the speleothem community and contextualize their interpretation in a regional framework for South America during the last two millennia. For that, we used only datasets that were available to us with speleothem $\delta^{13}C$ data from the last two thousand years (since year 0 CE). Therefore, we only consider this time period for the analyses presented here. All records used, including their references, cave names, locations and climatic parameters, are listed in Table 1. They are composed of 11,601 $\delta^{13}C$ data points from 25 speleothems, published in 15 different papers (Table 1).

3.2. Stalagmites and regional settings

As presented in the original papers, all speleothems used in this study were collected with the initial goal to reconstruct the SAMS using the $\delta^{18}O$ values. Therefore, stalagmites with a candle-type shape and uniform growth were preferentially collected in isolated chambers located far from the cave entrance. At such locations, temperature displays only minor variations throughout the year (characteristic of tropical caves), the air circulation is restricted, CO_2 concentrations are higher than atmospheric values, and the air is saturated in humidity. These conditions minimize the seasonal effects of ventilation and temperature, degassing and overall kinetic effects on the isotopic composition of the stalagmites.

The speleothem $\delta^{13}C$ records used here are distributed throughout tropical South America (Fig. 1), covering a region spanning the latitudes 4 °S to 21 °S and longitudes 42 °W to 76 °W. The domain comprises the following climates (according to the Köppen climate classification): monsoon (Am), tropical savanna (Aw), warm semi-arid (BSh) and humid subtropical (Cwa). The annual precipitation amount ranges from 450 to 2400 mm, mainly related to the SAMS and its subcomponent the SACZ (Novello et al., 2018). The equatorial portion is also under direct influence of the Intertropical Convergence Zone (ITCZ). Except for the sites located

Table 1
Caves, locations and regional characteristics. Information obtained from the original papers.

Stalagmite	Cave	Latitude °N	Longitude °E	Reference	Annual Precipitation (mm)	Mean annual T (°C)	Elevation (m.a.s.l)
JAR4	Jaraguá	−21.08	−56.58	Novello et al. (2018; 2019) This study	1400	21.4	570
JAR1	Jaraguá	−21.08	−56.58	Novello et al. (2018) This study	1400	21.4	570
SBE3	São Bernardo	−13.81	−46.35	Novello et al. (2018); Moquet et al. (2016) This study	1270	23.0	630
SMT5	São Matheus	−13.81	−46.35	Novello et al. (2018) This study	1270	23.0	630
ALHO6	Pau d'Alho	−15.21	−56.8	Novello et al. (2016) Jaqueto et al. (2016)	1440	25.5	340
CUR4	Curupira	−15.02	−56.78	Novello et al. (2016) This study	1440	25.5	340
DV2	Diva	−12.37	−41.57	Novello et al. (2012) This study	700	24.5	480
TR5	Torrinha	−12.37	−41.57	Novello et al. (2012) This study	700	24.5	480
LD12	Lapa Doce	−12.37	−41.57	Novello et al. (2012) This study	700	24.5	480
TRA7	Trapiá	−5.59	−37.70	Utida et al. (2020)	700	28.0	72
FN1	Furna Nova	−5.60	−37.44	Cruz et al. (2009) Utida et al. (2020)	700	28.0	100
TM0	Tamboril	−16.80	−47.27	Wortham et al. (2017)	1400	22.5	600
ANJOS1	Lapa dos Anjos	−14.39	−44.30	Stríkis (2015) This study	940	23.7	640
BTV21a	Botuverá	−27.21	−49.09	Bernal et al. (2016) This study	1400	22.0	200
PAR3	Paraiso	−4.07	−55.45	Wang et al. (2017)	2400	26.0	60
PAR1	Paraiso	−4.07	−55.45	Wang et al. (2017)	2400	26.0	60
MV3	Mata Virgem	−11.62	−47.49	Azevedo et al. (2019)	1570	26.8	365
POO-H1	Huagapo	−11.27	−75.79	Kanner et al. (2013)	459	10.4	3800
P09−H2	Huagapo	−11.27	−75.79	Kanner et al. (2013)	459	10.4	3800
BOTO3	Umajalanta −Chiflonkhakha	−18.12	−65.77	Apaéstegui et al. (2018) This study	518	17.0	2650
BOTO7	Umajalanta −Chiflonkhakha	−18.12	−65.77	Apaéstegui et al. (2018) This study	518	17.0	2650
BOTO10	Umajalanta −Chiflonkhakha	−18.12	−65.77	Apaéstegui et al. (2018) This study	518	17.0	2650
BOTO1	Umajalanta −Chiflonkhakha	−18.12	−65.77	Apaéstegui et al. (2018) This study	518	17.0	2650
PAL3	Palestina	−5.92	−77.35	Apaéstegui et al. (2014)	1570	22.8	870
PAL4	Palestina	−5.92	−77.35	Apaéstegui et al. (2014)	1570	22.8	870

in the Andes, all records are located at altitudes below 700 m.a.s.l. (Table 1). At these lowland sites, precipitation amount and the length of the rainy season define the three main vegetation types (Fig. 1). High precipitation amounts that are well distributed over the year are typical of Tropical Forest, while Caatinga is characterized by an environment with lower precipitation, concentrated during a few months. Cerrado, the main biome of central South America, presents hydrological conditions in-between these two end-members. In general, temperature decreases with increasing latitude and altitude; the mean annual temperature in the lowlands ranges from 21.4 to 26.8 °C, while the sites in the Andes reach temperatures around 10 °C (Table 1).

3.3. Methods

To assess the shared variance among the $\delta^{13}C$ records from the different cave sites, while considering the stalagmites' age uncertainties, we employ a Monte-Carlo Principal Component Analysis (MC-PCA) as described in Campos et al. (2019), which consists of the following steps: (1) A linear age-depth model was constructed for each record, accounting for the $\pm 1\sigma$ standard deviations in the dating uncertainty through a set of 1000 Monte-Carlo simulations, which resulted in 1000 age models for each isotopic sample. The corresponding isotopic time series are obtained through linear interpolation between ages using the age-depth model (Deininger et al., 2017); (2) Stalagmite records from the same karst region were merged into a single time series by synchronizing the time series using a cubic spline during the overlap period, and each time series was normalized to unit variance (z-scores) before they were averaged into one time series; (3) The time series were reconstructed using the inversion of the normalization of the longer time series (using standard deviation and the mean of the longer time series); (4) The time series were resampled to annual resolution before being low-pass filtered at the band of $1/30$ years^{-1}; (5) From the 1000 Monte-Carlo age model simulations, one time series is randomly chosen from each record, generating a set of time series; the Principal Component Analysis (PCA) is then performed over this set of data. This procedure is repeated 1000 times, in such a way that all the simulations are being used, generating a set of spatial patterns (or loadings), principal components (or scores) and eigenvalues (containing the explained variance of the spatial pattern and principal component). These analyses were carried out in Matlab with codes written using its native routines.

The MC-PCA was focused on the time period between 650 and 1950 CE because this is the time interval covered by most sites This procedure resulted in a set of ten time series, each corresponding to a site shown in Fig. 3: Jar (composed by JAR1 + JAR4), SBE (composed by SBE3 + SMT5), ALH (composed by ALHO6 + CUR4), DV2 (composed by DV2 + TR5 + LD12), TMO (composed only by TMO), ANJ (composed only by ANJOS1), PAR (composed by PAR1 + PAR3), HUA (composed by P00–H1 + P09–H2), BOTO (composed by BOTO1 + BOTO3 + BOTO7 +BOTO10) and PAL (composed by PAL3 + PAL4). Four stalagmites from sites presented in Fig. 1 (MV3, FN1, TRA7, BTV21a) were not included in the PCA because these records cover only a limited time period and no other stalagmites from the same karst systems exist that could be merged, or because their data resolution is significantly lower (more than 15 years between individual data points in the geochronological model).

Regression analyses between the $\delta^{13}C$ data and other parameters were performed using the data presented in Tables 1 and 2 to test possible climatic influences on the $\delta^{13}C$ values from stalagmites. Many stalagmites from this study are experience similar precipitation amounts and/or temperature. Hence, we used a single

averaged $\delta^{13}C$ value for the stalagmites that are located within regions that experience similar precipitation amount or temperature (listed in Table 1) to provide regression analysis tests: "$\delta^{13}C$ *vs.* precipitation amount" and "$\delta^{13}C$ *vs.* temperature". Precipitation and temperature values that fall within a range of 50 mm and 1 °C, respectively, were considered as similar. This approach results in one $\delta^{13}C$ value per climatic region entering the regression model, ensuring that climatic regions where stalagmites are more common are not overrepresented and therefore do not lead to regionally biased results. Sites from the high-altitude Andes (Umajalanta–Chiflonkhakha and Huagapo cave systems) were excluded in the correlation and regression analyses, as these sites introduce large outliers due to the differences in altitude and temperature, that would equally bias the results. The average $\delta^{13}C$ value over the last two millennia was used in the analysis, which allows us to use all stalagmites to provide a spatially more complete picture of the records from South America and minimize possible inconsistencies in the data related to geochronology and resolution. Restricting the analysis to only modern $\delta^{13}C$ values would be limiting the use of our dataset since only a few stalagmites present data from the last 50 years. In theory, the recent $\delta^{13}C$ values should be more closely related to current temperature and precipitation. However, as is shown in Fig. 2 and discussed in sections 4 and 5, using the $\delta^{13}C$ averaged over the full record still results in a high R^2 with high statistical significance ($p < 0.01$) for the relationship between $\delta^{13}C$ and climatic parameters, which suggest that average $\delta^{13}C$ values over the last two millennia are indeed representative of the current climatic conditions.

To establish the correlation between the $\delta^{13}C$ and the growth rate from speleothems, we calculated the growth rate based on the length of the interval between two consecutive U/Th ages and used the mean $\delta^{13}C$ value, averaged over the respective interval.

4. Results

The $\delta^{13}C$ values from the $\delta^{13}C\_2k\_SA$ dataset range from -11.5 to 6.8‰, although the vast majority of the data lie within -11 and -1‰ (Figs. 1–25 in supplementary material). The highest values and largest variability is from the TR5 stalagmite, ranging from -3.8 to 6.8‰ (amplitude of 10‰), which contrasts with the average amplitude of 4.5‰ from the other stalagmites.

The coefficient of determination (R^2) between the time series of $\delta^{18}O$ and $\delta^{13}C$ was calculated for each stalagmite and is listed in Table 2. The highest coefficient of determination (R^2: 0.96, $p < 0.01$) is displayed by the TR5 stalagmite, while the average R^2 of the $\delta^{13}C\_2k\_SA$ dataset is 0.29. Average $\delta^{13}C$ values from the speleothems display a high negative correlation with the annual mean precipitation amount (R^2: 0.67, $p < 0.01$) and a weaker, positive correlation with temperature (R^2: 0.45, $p < 0.05$) of their respective regions (Fig. 2). No significant correlation was found with altitude ($p > 0.05$). The relationships between the growth rate and average $\delta^{13}C$ values are statistically significant ($p \leq 0.05$) only in the stalagmites JAR4 (R^2: 0.21), DV2 (R^2: 0.50), TR5 (R^2: 0.75), LD12 (R^2: 0.70) and TRA7 (R^2: 0.20), all with negative slopes (Table 2).

The MC-PCA methodology was applied to the full $\delta^{13}C\_2k\_SA$ dataset. The first principal component (PC1) explained ~36% of the total variance (Figs. 3 and 4). Positive loadings are associated with the $\delta^{13}C$ records from the caves Huagapo (Hua), Palestina (PAL), Jaraguá (Jar), and the merged records from the caves Pau d'Alho/Curupira (Alh) and São Bernardo/São Matheus (SBE), whereas negative loadings are linked to the records from the caves Diva de Maura/Torrinha/Lapa Doce (DV2), Paraiso caves (PAR) and Umajalanta–Chiflonkhakha (BOTO) (Fig. 3), indicating out of phase $\delta^{13}C$ variability between the two cave site groups. Positive values

Table 2

Stalagmites and their respective data information. Coefficients of determination (R^2) between growth rate and $\delta^{13}C$ values was calculated based on the length interval between ages and the mean $\delta^{13}C$ values of each interval. Confidence levels at this column equal to or higher than 95% ($p \leq 0.05$) are shown in bold and the signal "+" and "-" denotes positive and negative slopes, respectively. (1) Novello et al. (2019); (2) Lima (2011); (3) Nogueira et al. (2006); (4) Caird et al. (2017); (5) Utida et al. (2020); (6) Alvarenga et al. (2014); (7) Caetano-Filho et al. (2019); (8) Campos (2013). (*) Site where the $\delta^{13}C$ values were measured in the bedrock that hosts the cave.

Stalagmite	$\delta^{18}O$ mean	$\delta^{13}C$ mean	R^2 $\delta^{18}O$ x $\delta^{13}C$	Time period covered (years BP)	Isotopic data points	Mean resolution (years)	R^2 Growth rate x $\delta^{13}C$	$\delta^{13}C$ of the main rock formation	Host geology
JAR4	−4.8	−8.5	0.50 (p < 0.01)	−50 to 760	237	3.4	(−) **0.21 (p=0.05)**, n° of segments: 18	1* (1)	Bocaina Fm, Corumba Group (Neoproterozoic)
JAR1	−3.8	−7.2	0.21 (p < 0.01)	499 to 1508	318	3.2	(+) 0.24 (p = 0.17), n° of segments: 9	1* (1)	Bocaina Fm Corumba Group (Neoproterozoic)
SBE3	−4.3	−8.9	0.04 (p < 0.01)	−60 to 827	1710	0.5	(+) 0.29 (p = 0.12), n° of segments: 10	−5.5 to −3 (2)	Urucuia Fm, Mata da Corda Group (Cretaceous)
SMT5	−4.2	−8.3	0.13 (p < 0.01)	749 to 1686	575	1.6	(−) 0.35 (p = 0.60), n° of segments: 3	−5.5 to −3 (2)	Urucuia Fm, Mata da Corda Group (Cretaceous)
ALHO6	−6.2	−6.6	0.57 (p < 0.01)	90 to 1458	1169	1.2	(+) 0.03 (p = 0.63), n° of segments: 11	−5 to 0 (3)	Guia Fm, Araras Group (Neoproterozoic)
CUR4	−7.6	−9.9	0.25 (p < 0.01)	−21 to 155	252	0.7	(+) 0.00 (p = 0.94), n° of segments: 7	−5 to 0(3)	Guia, Araras Group (Neoproterozoic)
DV2	−3.7	−9.2	0.35 (p < 0.01)	39 to 2765	538	5.0	(−) **0.50 (p=0.02)**, n° of segments: 10	−9 to +10 (4)	Salitre Fm, Una Group (Neoproterozoic)
TR5	−2.9	−1.1	0.96 (p < 0.01)	−57 to 76	90	1.5	(−) **0.75 (p<0.01)**, n° of segments: 7	−9 to +10 (4)	Salitre Fm, Uma Group (Neoproterozoic)
LD12	−3.2	−7.7	0.35 (p < 0.01)	−61 to 39	122	0.8	(−) **0.70 (p=0.04)**, n° of segments: 6	−9 to +10 (4)	Salitre Fm, Una Group (Neoproterozoic)
TRA7	−2.8	−3.0	0.05 (p < 0.01)	17 to 5507	818	6.4	(−)**0.20 (=0.03)**, n° of segments: 23	0* (5)	Jandaíra Fm, Apodi Group (Cretaceous)
FN1	−2.3	−4.9	0.87 (p < 0.03)	−54 to 2275	88	26.5	X, n° of segments: 3	0* (5)	Jandaíra Fm, Apodi Group (Cretaceous)
TM0	−5.4	−9.7	0.24 (p < 0.01)	−32 to 1678	471	3.6	0.00 (p = 0.87), n° of segments: 12	−5 to +16 (6)	Sete Lagos Fm, Bambui Group (Neoproterozoic))
ANJOS1	−3.7	−7.2	0.09 (p < 0.01)	−57 to 2927	1272	2.4	0.00 (p = 0.72), n° of segments: 26	−5 t0 +2 (7)	Sete Lagoas Fm. Bambúi Group (Neoproterozoic)
BTV21a	−3.8	−8.2	0.03 (p < 0.01)	196 to 9211	230	39.2	X, n° of segments: 3	X	Botuverá Fm, Brusque Group (Neoproterozoic)
PAR3	−5.7	−8.9	0.42 (p < 0.01)	−48 to 768	144	5.7	(−) 0.26 (p = 0.24), n° of segments: 7	−2.2 to 5.2 (8)	Itaituba Fm Tapajos Group (Paleozoic)
PAR1	−6.6	−9.5	0.00 (p < 0.44)	714 to 4812	449	9.1	X, n° of segments: 3	−2.2 to 5.2 (8)	Itaituba Fm Tapajos Group (Paleozoic)
MV3	−1.9	−4.7	0.45 (p < 0.01)	250 to 1032	537	1.4	(−) 0.46 (p = 0.10), n° of segments: 7	X	Mato Virgem Fm, Natividade Group (Precambrian)
P00−H1	−13.3	−5.9	0.24 (p < 0.01)	−50 to 1391	289	5.0	(+) 0.55 (p = 0.26), n° of segments: 4	X	Aramachay Fm, Pucara Group (Triassic)
P09−H2	−13.0	−5.2	0.20 (p < 0.01)	1099 to 7146	1272	5.7	(−) 0.35 (p = 0.29), n° of segments: 4	X	Aramachay Fm, Pucara Group (Triassic)
Boto3	−9.7	−1.7	0.26 (p < 0.01)	171 to 1242	256	4.0	(−) **0.94 (p=0.01)**, n° of segments: 8	X	Miraflores Fm, Pucara Group (Cretaceous)
Boto7	−10.8	−3.9	0.00 (p = 0.6)	78 to 388	97	1.8	X, n° of segments: 2	X	Miraflores Fm, Pucara Group (Cretaceous)
Boto10	−9.7	−3.1	0.34 (p < 0.01)	543 to 1217	207	3.3	(+) 0.36 (p = 0.40), n° of segments: 3	X	Miraflores Fm, Pucara Group (Cretaceous)
Boto1	−10.2	−1.2	0.41 (p < 0.01)	218 to 383	20	7.9	X, n° of segments: 1	X	Miraflores Fm, Pucara Group (Cretaceous)
PAL3	−7.1	−10.1	0.00 (p = 0.2)	21 to 850	192	4.3	(+) 0.65 (p = 0.10), n° of segments: 4	X	Chambara Fm, Pucara Group (Triassic_Jurassic)
PAL4	−7.1	−9.4	0.25 (p < 0.01)	151 to 1536	248	5.4	(+) 0.12 (p = 0.27), n° of segments: 11	X	Chambara Fm, Pucara Group (Triassic_Jurassic)

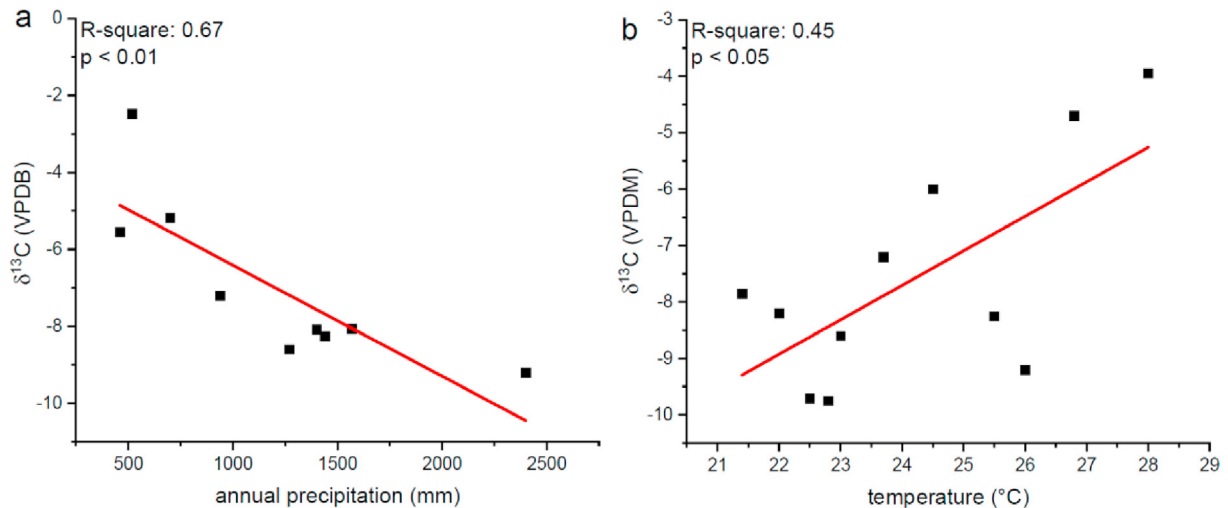**Fig. 2.** Relationship between the $\delta^{13}C$ from the $\delta^{13}C\_2k\_SA$ dataset with annual precipitation (a) and annual mean temperature (b) of each study site.
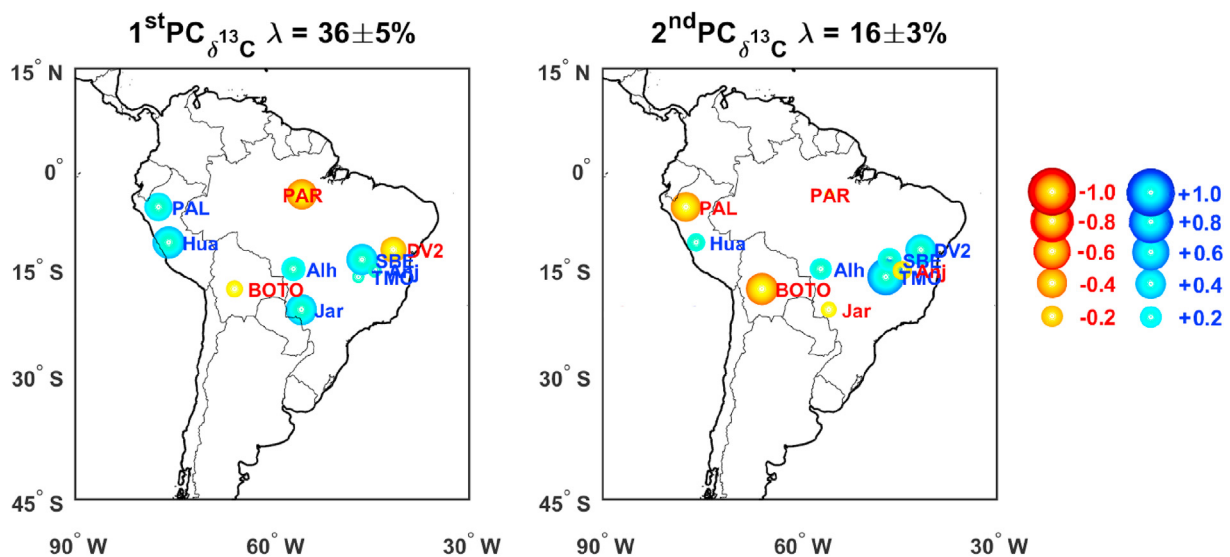

Fig. 3. Maps of South America with the main loadings of the Principal Component Analysis (PCA) and explained total variance. Blue and red dots represent positive and negative loadings, respectively. The magnitude of the loadings is represented by the size of the dots. The larger the dot, the more representative it's loading is of the respective PC. (For interpretation of the references to color in this figure legend, the reader is referred to the Web version of this article.)

characterize the time interval of ~600−1500 CE in PC1, while negative values are predominant during the period ~1500−1950 CE, with an incursion to more negative values centered at ~1180 CE (Fig. 4). PC2 explained ~16% of the variance, with large positive loadings displayed by the records located in central Brazil, especially the TM0 and DV2 records, whereas large negative loadings are displayed by the records from high altitudes (PAL and BOTO). The other study sites present low and variable contributions for PC2.

5. Discussion

The host-rocks of the caves in this study are predominantly of Neoproterozoic age, located in the Brazilian shield (Table 2). Isotopic studies carried out in these carbonate rock sequences show a wide range of values, varying between ~ −5 to 16‰ within the same rock unit or even the same outcrop (Table 2). The absence of isotopic studies in the same bedrock where the caves are located,

precludes a precise quantification of the influence of these different rock sequences on the $\delta^{13}C$ values of the stalagmites. Of the study sites presented here, the $\delta^{13}C$ from its host-rock was only measured at Jaraguá and Trapiá caves (Novello et al., 2019; Utida et al., 2020). In both sites, more positive $\delta^{13}C$ values close to bedrock values were reported in their stalagmites during periods of sparse vegetation and thin soil layers above the caves. Although both papers are describing environmental changes at orbital timescales, nowadays these are the typical characteristics of the sites Huagapo, Umajalanta−Chiflonkhakha, Mata Virgem, Trapiá and Torrinha; all featuring stalagmites with high $\delta^{13}C$ values (Table 2). Aside from the stalagmites of these sites and ALHO6, all other stalagmites have $\delta^{13}C$ values lower than −6‰ throughout the last two millennia, indicating the predominance of thick soil with higher organic matter content from the regions of Cerrado and/or Tropical Forest. $\delta^{13}C$ values below −6‰ in stalagmites are also considered indicative of predominance of C$_3$ plants above the caves in geochemical models (McDermott, 2004; Baker et al., 1997; Dreybrodt, 1988), if
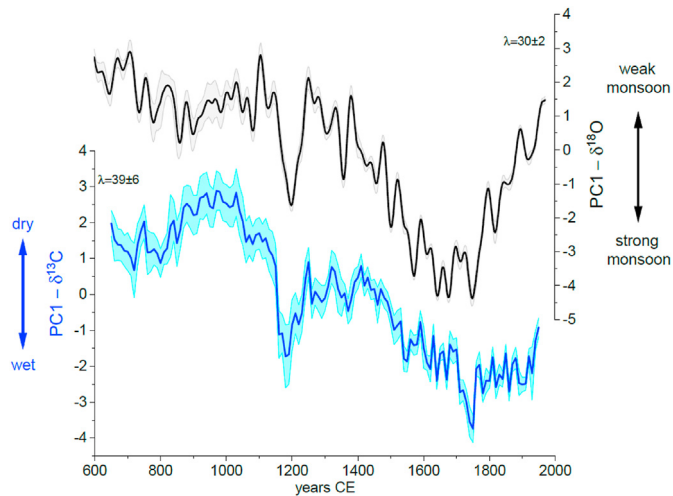
Fig. 4. Comparison between the first Principal Component (PC1) derived from the δ¹³C_2k_SA dataset (this study) representing the main mode of hydroclimate variability and PC1 based on the δ¹⁸O from stalagmites from South America (PC1 − δ¹⁸O) from Campos et al. (2019) representing the main mode of variability of the South American Monsoon System. The uncertainties associated with the PC1s are shown by the colored and gray shading. λ indicates the percentage of explained variance by each PC.

considering bedrock with δ¹³C values around +1‰ (which is the average value for South American carbonates, Table 2).

TR5 presents δ¹³C values that are significantly higher than all other samples, and the abrupt increase in δ¹³C occurs just before the complete stop of carbonate deposition at ~1920 CE and ~2006 CE, both of which are periods of predominantly dry conditions in the region (Novello et al., 2012). High values followed by an abrupt decrease also occur after the depositional hiatus at ~1960 CE. The R^2 between δ¹³C and δ¹⁸O is close to 1 (Table 2), which indicates that both isotopes underwent fractionation together in this sample. These results support the notion that the TR5 stalagmite was precipitated under strong kinetic effects due to high evaporation rates and/or significantly reduced dripping rates (resulting in a long time period for isotope re-equilibration between solution and cave atmosphere) at the moment of carbonate precipitation, which is accentuated during drier periods, culminating in a complete halt of carbonate precipitation. Although the kinetic effect might be the main factor responsible for the high amplitude and isotopic values in TR5, this stalagmite still preserves paleoclimate information regarding the δ¹⁸O in precipitation that co-varies with the δ¹⁸O from other stalagmites in the region, as well as with pluviometric data from meteorological stations (Novello et al., 2012).

Most of the stalagmites from the δ¹³C_2k_SA dataset feature R^2 between their δ¹³C and δ¹⁸O values ranging from 0.20 to 0.56 (Table 2). The δ¹⁸O values in stalagmites from tropical South America covering the last 2000 years have been interpreted as a proxy of the intensity of the SAMS (Azevedo et al., 2019; Novello et al., 2012, 2016, 2018, 2018; Apaéstegui et al., 2014, 2018; Wortham et al., 2017; Vuille et al., 2012) and the SACZ, a continuous band of low-level wind convergence and precipitation that extends in a northwest-southeast direction across southeastern South America (Novello et al., 2018). Since an increase in local rainfall promotes a decrease of PCP, an increase of gas CO_2 derived from soil organic matter and favors C_3 plants over C_4 plants (all processes that result in decreasing δ¹³C values in stalagmites), we argue that a correlation between δ¹³C and δ¹⁸O values is the result of a close relationship between local hydroclimate and atmospheric convective processes (inferred by δ¹⁸O). This hypothesis is supported by

the existing correlation between the annual rainfall amount and the average δ¹³C values of the stalagmites (R^2: 0.67, Fig. 2), and by the PC1 loadings derived from the δ¹³C_2k_SA dataset (Fig. 3), showing a very similar spatial distribution as those displayed in PC1 derived from the δ¹⁸O dataset from speleothems over tropical South America by Campos et al. (2019). Both PC1-δ¹³C and PC1-δ¹⁸O show positive loadings for the locations to the southwest of the SACZ and negatives loadings for those records located to the northeast (Fig. 3), which characterizes the SACZ precipitation dipole in South America (Campos et al., 2019; Novello et al., 2018). The BOTO site (Fig. 3) is an exception in this scenario, but this region may have partially been under the influence from a different climate system with a different moisture source in the past (Apaéstegui et al., 2018). This relationship between the δ¹³C and local hydroclimate was already documented for the ALHO6 stalagmite using a multiproxy approach (Jaqueto et al., 2016).

Strong correspondence throughout the time-series between scores of PC1-δ¹³C and PC1-δ¹⁸O further corroborates the overall coupling between the monsoon and local hydroclimate during the last ~1400 years (Fig. 4). This coupling ceases after ~1750 CE, when the monsoon weakened at a faster rate than the local hydrological response. However, the hydrologic variability inferred from PC1-δ¹³C is biased by vegetation changes, which responds to other influences beyond the local rainfall amount, such as temperature, atmospheric CO_2, deforestation and fire (parameters that have increased significantly over the last 250 years).

PC2 explains only 16% of the δ¹³C variability (Fig. 3). It shows large positive loadings at sites located in lowlands of central Brazil and negative loadings at sites located in the Andes (Fig. 3). This difference is possibly related to different effects of temperature at different altitudes. Changes in continental temperature are amplified at higher elevation (Ohmura, 2012), leading to a larger effect on the δ¹³C values at sites located at higher altitudes, thereby increasing the isotopic differences between sites located at low and high elevation.

Growth rates also show a weak correlation with the δ¹³C values from the δ¹³C_2k_SA dataset. The correlation between the growth rate and δ¹³C values is statistically significant (p-values ≤ 0.05) only in the stalagmites JAR4, DV2, TR5, LD12 and TRA7 (Table 2). In these stalagmites, all regression coefficients present a negative slope, which is expected, as a higher growth rate leads to lower δ¹³C values because the time for isotopic enrichment of the DIC through kinetic effects is reduced during carbonate precipitation (Fohlmeister et al., 2020).

6. Conclusions

Here we present a new set of δ¹³C records from speleothems collected over a broad region of tropical South America. These data were integrated with previously published speleothem δ¹³C records to characterize the main controls on carbon isotope variations in this region. The predominance of C_3 plants above most of the karst systems studied here is responsible for the low δ¹³C values (<−6‰) in most of the speleothems, while local hydroclimate associated with PCP process is the main driver behind its variability during the last two millennia. Unlike what was observed in the global compilation of δ¹³C records for the period after 1900 CE (Fohlmeister et al., 2020), local temperature and growth rate play a minor role in shaping the δ¹³C values in the δ¹³C_2k_SA dataset. The probable reason for this difference between studies is that most of the speleothems in our database formed under tropical conditions, characterized by a limited temperature range, whereas the SISAL_v1 dataset studied by Fohlmeister et al. (2020) is biased towards records from high latitudes with a much larger temperature

range.

Using Monte Carlo Principal Component Analysis, we produce an index of the mean hydrologic conditions and its changes over tropical South America for the last two millennia, which is closely related to monsoon variability for the period prior to 1750 CE. The recent break-down in the relationship between monsoon and local hydroclimate may have been caused by the increase in temperature, CO_2, deforestation and fire during the current warm period; however, further studies are required to test this hypothesis.

Data availability

The new $\delta^{13}C$ records from $\delta^{13}C\_2k\_SA$ dataset will be available at PANGAEA (https://doi.pangaea.de/10.1594/PANGAEA.924810).

Author contribution

VFN designed the experiments, FWC and MV are the project PIs, JLPSC performed statistical analysis, NMS and JSM performed isotopic analyses, VA, GU, PJ, IK, LCRP and DOB assisted in the discussion and interpretations. AA created the map, GMPS provided a review on carbonate formations. VFN prepared the manuscript with contributions from all co-authors.

Declaration of competing interest

The authors declare that they have no known competing financial interests or personal relationships that could have appeared to influence the work reported in this paper.

Acknowledgements

Appendix A. Supplementary data

Supplementary data to this article can be found online at https://doi.org/10.1016/j.quascirev.2021.106822.

References

Alvarenga, C.J.S., Santos, R.V., Vieira, L.C., Lima, Barbara A.F., Mancini, L.H., 2014. Meso-Neoproterozoic isotope stratigraphy on carbonates platforms in the Brasilia Belt of Brazil. Precambrian Res. 251, 164−180. https://doi.org/10.1016/j.precamres.2014.06.011.

Apaéstegui, J., Cruz, F.W., Vuille, M., Fohlmeister, J., Espinoza, J.C., Sifeddine, A., Strikis, N., Guyot, J.L., Ventura, R., Cheng, H., Edwards, R.L., 2018. Precipitation changes over the eastern Bolivian Andes inferred from speleothem (d18O) records for the last 1400 years. Earth Planet Sci. Lett. 494, 124−134. https://doi.org/10.1016/j.epsl.2018.04.048.

Apaéstegui, J., Cruz, F.W., Sifeddine, A., Vuille, M., Espinoza, J.C., Guyot, J.-L., Khodri, M., Strikis, N., Santos, R.V., Cheng, H., Edwards, L., Carvalho, E., Santini, J., 2014. Hydroclimate variability of the northwestern Amazon Basin near the Andean foothills of Peru related to the South American Monsoon System during the last 1600 years. Clim. Past 10. https://doi.org/10.5194/cp-10-1967-2014, 1967−1981.

Azevedo, V., Stríkis, N.M., Santos, R.A., Souza, J.G., Ampuero, A., Cruz, F.W., Oliveira, P., Stumpf, C.F., Vuille, M., Mendes, V.R., Cheng, H., Edwards, R.L., 2019. Medieval Climate Variability in the eastern Amazon-Cerrado regions and its archeological implications. Sci. Rep. 9, 20306. https://doi.org/10.1038/s41598-019-56852-7.

Badeck, F.W., Tcherkez, G., Nogues, S., Piel, C., Ghashghaie, J., 2015. Post-photosynthetic fractionation of stable carbon isotopes between plant organs—a widespread phenomenon. Rapid Commun. Mass Spectrom. 19 (11), 1381−1391.

https://doi.org/10.1002/rcm.1912.

Baker, A., Ito, E., Smart, P.L., McEwan, R.F., 1997. Elevated and variable values of d13C in speleothems in a British cave system. Chem. Geol. 136, 263−270.

Baldini, J.U.L., McDermott, F., Hoffmann, D.L., Richards, D.A., Clipson, N., 2008. Very high-frequency and seasonal cave atmosphere PCO2 variability: implications for stalagmite growth and oxygen isotope-based paleoclimate records. Earth Planet Sci. Lett. 272, 118−129. https://doi.org/10.1016/j.epsl.2008.04.031.

Bernal, J.P., Cruz, F.W., Stríkis, N.M., Wang, X., Deininger, M., Catunda, M.C.A., Ortega-Obregón, C., Cheng, H., Edwards, R.L., Auler, A.S., 2016. High-resolution Holocene south American monsoon history recorded by a speleothem from Botuverá cave, Brazil. Earth Planet Sci. Lett. 450, 186−196. https://doi.org/10.1016/j.epsl.2016.06.008.

Bird, B.W., Abbott, M.B., Vuille, M., Rodbell, D.T., Stansell, N.D., Rosenmeier, M.F., 2011. A 2,300-year-long annually resolved record of the South American summer monsoon from the Peruvian Andes. Proc. Natl. Acad. Sci. Unit. States Am. 108 (21), 8583−8588. https://doi.org/10.1073/pnas.1003719108.

Breecker, D.O., 2017. Atmospheric pCO2 control on speleothem stable carbon isotope compositions. Earth Planet Sci. Lett. 458, 58−68. https://doi.org/10.1016/j.epsl.2016.10.042.

Caetano-Filho, S., Paula-Santos, G.M., Guacaneme, C., Babinski, M., Babinski, M., Bedoya-Rueda, C., Peloso, M., Amorim, K., Afonso, J., Kuchenbecker, M., Reis, H.L.S., Trindade, R.I.F., 2019. Sequence stratigraphy and chemostratigraphy of an Ediacaran-Cambrian foreland-related carbonate ramp (Bambuí Group, Brazil). Precambrian Res. 331, 105365. https://doi.org/10.1016/j.precamres.2019.105365.

Caird, R.A., Pufahl, P.K., Hiatt, E.E., Abram, M.B., Rocha, A.J.D., Kyser, T.K., 2017. Ediacaran stromatolites and intertidal phosphorite of the salitre formation, Brazil: phosphogenesis during the neoproterozoic oxygenation event. Sediment. Geol. 350, 55−71. https://doi.org/10.1016/j.sedgeo.2017.01.005.

Calo, C.M., Cortés, L.I., 2009. A contribution to the study of diet of formative societies in Northwestern Argentina: isotopic and archaeological evidence. Int. J. Osteoarchaeol. 19, 192−203. http://doi:10.1002/oa.1052.

Campos, A.C.P.P., 2013. Paleoambiente e quimioestratigrafia da formação Itaituba, carbonífero da borda sul da Bacia do Amazonas, região de Uruará − Pará. Amélia Carolina Pimenta Parente de Campos. M. S. thesis. Universidade Federal do Pará, Brazil, p. 77, 2013.

Campos, J.L.P.S., Cruz, F.W., Ambrizzi, T., Deininger, M., Vuille, M., Novello, V.F., Stríkis, N.M., 2019. Coherent South American monsoon variability during the last millennium revealed through high-resolution proxy records. Geophys. Res. Lett. 46, 8261−8270. https://doi.org/10.1029/2019GL082513.

Cerling, T.E., 1984. The stable isotopic composition of modern soil carbonate and its relationship to climate. Earth Planet Sci. Lett. 71 (2), 229−240. https://doi.org/10.1016/0012-821X(84)90089-X.

Cruz, F.W., Burns, S.J., Jercinovic, M., Karmann, I., Sharp, W.D., Vuille, M., 2006. Evidence of rainfall variations in Southern Brazil from trace element ratios (Mg/Ca and Sr/Ca) in a Late Pleistocene stalagmite. Earth Planet Sci. Lett. 71, 2250−2263. http://doi:10.1016/j.gca.2007.02.005.

Cruz, F.W., Vuille, M., Burns, S.J., Wang, X., Cheng, H., Werner, M., Edwards, R.L., Karmann, I., Auler, A.S., Nguyen, H., 2009. Orbitally driven east-west anti-phasing of South American precipitation. Nat. Geosci. 2, 210−214. http://doi:10.1038/NGEO0444.

Deininger, M., McDermott, F., Mudelsee, M., Werner, M., Frank, N., Mangini, A., 2017. Coherency of late Holocene European speleothem δ18O records linked to North Atlantic Ocean circulation. Clim. Dynam. 49 (1-2), 595−618. https://doi.org/10.1007/s00382-016-3360-8.

Dreybrodt, W., 1988. Processes in Karst Systems. Springer Series in Physical Environment. Springer, Heidelberg.

Ehleringer, J.R., Cerling, T.E., Helliker, B.R., 1997. C4 photosynthesis, atmospheric CO2, and climate. Oecologia 112, 285−299. https://doi.org/10.1007/s004420050311.

Fairchild, I.J., Baker, A., 2012. Speleothem Science: from Process to Past Environments. Wiley-Blackwell.

Fohlmeister, J., Voarintsoa, N.R.G., Lechleitner, F.A., Boyd, M., Brandstätter, S., Jacobson, M.J., Oster, J., 2020. Main controls on the stable carbon isotope composition of speleothems. Geochem. Cosmochim. Acta GCA11710. https://doi.org/10.1016/j.gca.2020.03.042.

Fohlmeister, J., Scholz, D., Kromer, B., Mangini, A., 2011. Modelling carbon isotopes of carbonates in cave drip water. Geochem. Cosmochim. Acta 75 (18), 5219−5228. https://doi.org/10.1016/j.gca.2011.06.023.

Hartman, G., Danin, A., 2010. Isotopic values of plants in relation to water availability in the Eastern Mediterranean region. Oecologia 162, 837−852. https://doi.org/10.1007/s00442-009-1514-7.

Hendy, C.H., 1971. The isotopic geochemistry of speleothems 1. The calculation of the effects of the different modes of formation on the isotopic composition of speleothems and their applicability as palaeoclimatic indicators. Geochem. Cosmochim. Acta 35, 801−824. https://doi.org/10.1016/0016-7037(71)90127-X.

Huffman, G., Bolvin, D.T., Braithwaite, D., Hsu, K., Joyce, R., Xie, P., 2014. Integrated Multi-satellitE Retrievals for GPM (IMERG), Version 4.4. NASA's Precip. Process. Cent.

Jaqueto, P., Trindade, R.I.F., Hartmann, G.A., Novello, V.F., Cruz, F.W., Karmann, I., Strauss, B.E., Feinberg, J.M., 2016. Linking speleothem and soil magnetism in the Pau d'Alho cave (central South America). J. Geophys. Res. Solid. Earth 121. http://doi:10.1002/2016JB013541.

Jia, G., Shevliakova, E., Artaxo, P., De Noblet-Ducoudré, N., Houghton, R., House, J., Kitajima, K., Lennard, C., Popp, A., Sirin, A., Sukumar, R., Verchot, L., 2019. Land−climate interactions. In: Shukla, P.R., Skea, J., Calvo Buendia, E., Masson-

Delmotte, V., Pörtner, H.-O., Roberts, D.C., Zhai, P., Slade, R., Connors, S., Van Diemen, Ferrat, R.M., Haughey, E., Luz, S., Neogi, S., Pathak, M., Petzold, J., Portugal Pereira, J., Vyas, P., Huntley, E., Kissick, K., Belkacemi, M., Malley, J. (Eds.), Climate Change and Land: an IPCC Special Report on Climate Change, Desertification, Land Degradation, Sustainable Land Management, Food Security, and Greenhouse Gas Fluxes in Terrestrial Ecosystems. https://www.ipcc.ch/srccl/chapter/chapter-2/.

Kanner, L.C., Burns, S.J., Cheng, H., Edwards, R.L., Vuille, M., 2013. High-resolution variability of the South American summer monsoon over the last seven millennia: insights from a speleothem record from the central Peruvian Andes. Quat. Sci. Rev. 75, 1–10. https://doi.org/10.1016/j.quascirev.2013.05.008.

Lachniet, M.S., 2009. Climatic and environmental controls on speleothem oxygen-isotope values. Quat. Sci. Rev. 28, 412–432. https://doi.org/10.1016/j.quascirev.2008.10.021.

Lima, O.N.B., 2011. Estratigrafia isotópica e evolução sedimentar do Grupo Bambuí na borda ocidental do Cráton do São Francisco: implicação tectônica e paleoambiental. Ph.D. thesis, Universidade de Brasilia, Brazil, p. 114, 2011.

McDermott, F., 2004. Palaeo-climate reconstruction from stable isotope variations in speleothems: a review. Quat. Sci. Rev. 23, 901–918. https://doi.org/10.1016/j.quascirev.2003.06.021.

Mickler, P.J., Carlson, P., Banner, J.L., Breecker, D.O., Stern, L., Guilfoyle, A., 2019. Quantifying carbon isotope disequilibrium during in-cave evolution of drip water along discreet flow paths. Geochem. Cosmochim. Acta 244, 182–196. https://doi.org/10.1016/j.gca.2018.09.027.

Mickler, P.J., Stern, L.A., Banner, J.L., 2006. Large Kinect isotope effects in modern speleothems. Geol. Soc. Am. Bull. 118, 65–81. https://doi.org/10.1130/B25698.1.

Moquet, J.S., Cruz, F.W., Novello, V.F., Stríkis, N.M., Deininger, M., Karmann, I., Santos, R.V., Millo, C., Apaestegui, J., Guyot, J.-L., Siffedine, A., Vuille, M., Cheng, H., Edwards, R.L., Santini, W., 2016. Calibration of speleothem d18O records against hydroclimate instrumental records in Central Brazil. Global Planet. Change 139, 151–164. https://doi.org/10.1016/j.gloplacha.2016.02.001.

Nogueira, A.C.R., Riccomini, C., 2006. O Grupo Araras (Neoproterozóico) na parte norte da faixa Paraguai e sul do craton amazônico, Brasil. Braz. J. Genet. 36, 576–587.

Novello, V.F., Cruz, F.W., Karmann, I., Burns, S.J., Stríkis, N.M., Vuille, M., Cheng, H., Edwards, R.L., Santos, R.V., Frigo, E., Barreto, E.A.S., 2012. Multidecadal climate variability in Brazil's Nordeste during the last 3000 years based on speleothem isotope records. Geophys. Res. Lett. 39, L23706. https://doi.org/10.1029/2012GL053936.

Novello, V.F., Vuille, M., Cruz, F.W., Stríkis, N.M., Saito de Paula, M., Edwards, R.L., Cheng, H., Karmann, I., Jaqueto, P.F., Trindade, R.I.F., Hartmann, G.A., Moquet, J.S., 2016. Centennial-scale solar forcing of the South American Monsoon System recorded in stalagmites. Sci. Rep. 6, 24762. https://doi.org/10.1038/srep24762.

Novello, V.F., Cruz, F.W., Moquet, J.S., Vuille, M., de Paula, M.S., Nunes, D., Edwards, R.L., Cheng, H., Karmann, I., Utida, G., Stríkis, N.M., Campos, J.L.P.S., 2018. Two millennia of South Atlantic Convergence Zone variability reconstructed from isotopic proxies. Geophys. Res. Lett. 45 https://doi.org/10.1029/2017GL076838.

Novello, V.F., Cruz, F.W., McGlue, M.M., Wong, C.I., Ward, B.M., Vuille, M., Santos, R.A., Jaqueto, P., Pessenda, L.C.R., Atorre, T., Ribeiro, L.M.A.L., Karmann, I., Barreto, E.S., Cheng, H., Edwards, R.L., Paula, M.S., Scholz, D., 2019. Vegetation and environmental changes in tropical South America from the last glacial to the Holocene documented by multiple cave sediment proxies. Earth Planet Sci. Lett. 524, 115717. https://doi.org/10.1016/j.epsl.2019.115717.

Ohmura, A., 2012. Enhanced temperature variability in high-altitude climate change. Theor. Appl. Climatol. 110, 499–508. https://doi.org/10.1007/s00704-012-0687-x.

Olson, D.M., Dinerstein, E., Wikramanayake, E.D., Burgess, N.D., Powell, G.V.N., Underwood, E.C., D'amico, J.A., Itoua, I., Strand, H.E., Morrison, J.C., Loucks, C.J., Allnut, T.F., Ricketts, T.H., Kura, Y., Lamoreus, J.F., Wettengel, W.W., Hedao, P., Kassem, K.R., 2001. Terrestrial ecoregions of the world: a new map of life on earth. Bioscience 51, 933–938. https://doi.org/10.1641/0006-3568(2001)051[0933:TEOTWA]2.0.CO;2.

Pansani, T.R., Muniz, F.P., Cherkinsky, A., Pacheco, M.L.A.F., Dantas, M.A.T., 2019. Isotopic paleoecology ($\delta^{13}C$, $\delta^{18}O$) of late quaternary megafauna from mato grosso do sul and bahia states, Brazil. Quat. Sci. Rev. 221, 105864. https://doi.org/10.1016/j.quascirev.2019.105864.

Pessenda, L.C.R., Gouveia, S.E.M., Ribeiro, A.S., Oliveira, P.E., Aravena, R., 2020. Late Pleistocene and Holocene vegetation changes in northeastern Brazil determined from carbon isotopes and charcoal records in soil. Palaeogeogr. Palaeocl. 297, 597–608. https://doi.org/10.1016/j.palaeo.2010.09.008.

Polag, D., Scholz, D., Mühlinghaus, C., Spötl, C., Schröder-Ritzrau, A., Segl, M., Mangini, A., 2010. Stable isotope fractionation in speleothems: laboratory experiments. Chem. Geol. 279, 31–39. https://doi.org/10.1016/j.chemgeo.2010.09.016.

Quade, J., Cerling, T.E., Bowman, J.R., 1989. Systematic variations in the carbon and oxygen isotopic composition of pedogenic carbonate along transects in the Southern Great Basin, United States. Geol. Soc. Am. Bull. 101, 464–475. https://doi.org/10.1130/0016-7606(1989)101<0464:SVITCA>2.3.CO;2.

Rayner, P.J., Enting, I.G., Francey, R.J., Langenfelds, R., 1999. Reconstructing the recent carbon cycle from atmospheric CO_2, $\delta^{13}C$ and O_2/N_2 observations. Tellus B 51 (2), 213–232. https://doi.org/10.3402/tellusb.v51i2.16273.

Reuter, J., Stott, L., Khider, D., Sinha, A., Cheng, H., Edwards, R.L., 2009. A new perspective on the hydroclimate variability in northern South America during the Little Ice Age. Geophys. Res. Lett. 36, L21706. https://doi.org/10.1029/2009GL041051.

Schubert, B.A., Jahren, A.H., 2012. The effect of atmospheric CO_2 concentration on carbon isotope fractionation in C_3 land plants. Geochem. Cosmochim. Acta 96, 29–43. https://doi.org/10.1016/j.gca.2012.08.003.

Stríkis, N.M., 2015. Atividade do Sistema de Monção Sul-americana na porção central do Brasil durante o último período glacial a partir da aplicação de isótopos de oxigênio em espeleotemas. Ph.D. thesis. Instituto de Geociências, Universidade de São Paulo, Brazil, p. 265.

Utida, G., Cruz, F.W., Santos, R.V., Sawakuchi, A.O., Wang, H., Pessenda, L.C.R., Novello, V.F., Vuille, M., Stríkis, N.M., Guedes, C., Cheng, H., Edwards, R.L., 2020. Climate changes in Northeastern Brazil from Deglacial to Meghalayan periods and related environmental impacts. Quat. Sci. Rev. 250, 106655. https://doi.org/10.1016/j.quascirev.2020.106655.

Van de Water, P.K., Leavitt, S.W., Betancourt, J.L., 1994. Trends in stomatal density and 13C/12C ratios of Pinus flexilis needles during last glacial-interglacial cycle. Science 264 (5156), 239–243.

Vuille, M., Burns, S.J., Taylor, B.L., Cruz, F.W., Bird, B.W., Abbott, M.B., Kanner, L.C., Cheng, H., Novello, V.F., 2012. A review of the South American Monsoon history as recorded in stable isotopic proxies over the past two millennia. Clim. Past 8 (4), 1309–1321. https://doi.org/10.5194/cp-8-1309-2012.

Wang, X., Edwards, R.L., Auler, A.S., Cheng, H., Kong, X., Wang, Y., Cruz, F.W., Dorale, J.A.D., Chiang, H.-W., 2017. Hydroclimate changes across the Amazon lowlands over the past 45,000 years. Nature 541, 204–209. https://doi.org/10.1038/nature20787.

Wortham, B.E., Wong, C.I., Silva, L.C.R., McGee, D., Montañez, I.P., Rasbury, E.T., Cooper, K.M., Sharp, W.D., Glessner, J.J.G., Santos, R.V., 2017. Assessing response of local moisture conditions in central Brazil to variability in regional monsoon intensity using speleothem $^{87}Sr/^{86}Sr$ values. Earth Planet Sci. Lett. 463, 310–322. https://doi.org/10.1016/j.epsl.2017.01.034.